Applied Catalysis B: Environmental 245 (2019) 753–759

Contents lists available at ScienceDirect

Applied Catalysis B: Environmental

journal homepage: www.elsevier.com/locate/apcatb

Solvent-free method to encapsulate polyoxometalate into metal-organic frameworks as efficient and recyclable photocatalyst for harmful sulfamethazine degrading in water

Gaopeng Li[a,1], Kun Zhang[b,1], Chengbo Li[a], Ruicheng Gao[a], Yongliang Cheng[a], Lei Hou[a,*], Yaoyu Wang[a,*]

[a] Key Laboratory of Synthetic and Natural Functional Molecule Chemistry of the Ministry of Education, Shaanxi Key Laboratory of Physico-Inorganic Chemistry, College of Chemistry & Materials Science, Northwest University, Xi'an 710127, PR China
[b] School of Textile Science and Engineering, Xi'an Polytechnic University, Xi'an 710048, PR China

ARTICLE INFO

Keywords:
Solvent-free
Metal-organic framework
Polyoxometalate
Photocatalytic materials
Sulfamethazine

ABSTRACT

Through a less-investigated *in-situ* hot-pressing synthesis method, the phosphotungstic acid $H_3PW_{12}O_{40}$ (denoted as PW_{12}) was rapidly incorporated into a metal-organic framework MFM-300(In) in a short time, affording novel PW_{12}@MFM-300(In) composites. This solvent-free preparation process is not only environment-friendly but also energy/time-saving. The inclusion of PW_{12} in MFM-300(In) was demonstrated by different physical and chemical characterizations. It was interesting to find that PW_{12}@MFM-300(In) as new heterocatalysts display synergistic activity for the visible-light-driven catalytic degradation of pharmaceutically active compound sulfamethazine (SMT). 4-PW_{12}@MFM-300(In) with excellent robustness possesses the high removal efficiency of about 98% toward SMT within 2 h at room temperature, and can also be recycled multiple times for this catalytic process.

1. Introduction

The waste of pharmaceutically active compounds (PhACs) as common pollutants have become an urgent issue garnering the attentions of public and scientists, due to their pseudo-persistence, potential toxic effects on microorganisms, and widespread occurrence in surface waters [1–3]. Recent studies have revealed that the municipal wastewater treatment plant (WWTP) effluent is the main contributor of PhACs loadings to the ecosystem because the conventional wastewater biological treatment processes are not ideal for removing these pollutants [4–6]. To address this issue, various physical and chemical methods have recently been investigated, such as activated carbon adsorption, membrane filtration as well as advanced oxidation processes. Among those, photocatalysis is a promising technique considering its low energy consumption, mild operation condition and little production of byproducts [7–11].

Polyoxometalates (POMs) that possess unique anionic early transition metal-oxygen clusters and excellent acid/oxidation catalytic properties have shown great application prospects as photocatalysts [12–17]. Nevertheless, the utilization of independent POMs in catalysis reactions was constrained by their low specific surface areas as solid catalysts or difficult regeneration as homogeneous catalysts [18,19]. In contrast, the immobilization of POMs in various supports possessing high surface areas has been proposed as a cute strategy to design and manipulate active sites at molecular and atomic levels [20–25]. As a type of porous materials, metal-organic frameworks (MOFs) have attracted considerable attention of researchers due to which offer a potential platform for anchoring photosensitizers and catalytic moieties [26,27]. Heterogenizing POMs into MOFs to generate POM@MOF composites was developed as an important breakthrough in this regard because MOFs offer regular pore sizes, suitable voids and large surface areas [26,28–38]. In those reports, POMs were immobilized into appropriate MOFs by means of solvothermal synthesis to form POM@MOF composites, in which the POMs are orderly arranged in pores, and the composites reveal excellent catalytic efficiency toward various substrates [9,19,31,39]. Unfortunately, the preparation process of those materials is always accompanied by some undesirable problems, including the massive utilization of organic solvents, high reaction temperatures, long reaction times, a large excess of POMs, and low loading efficiency. Therefore, the development of facile and environment-

* Corresponding authors.
E-mail addresses: lhou2009@nwu.edu.cn (L. Hou), wyaoyu@nwu.edu.cn (Y. Wang).
[1] These authors contribute equally to this work.

https://doi.org/10.1016/j.apcatb.2019.01.012
Received 10 October 2018; Received in revised form 25 December 2018; Accepted 6 January 2019
Available online 07 January 2019

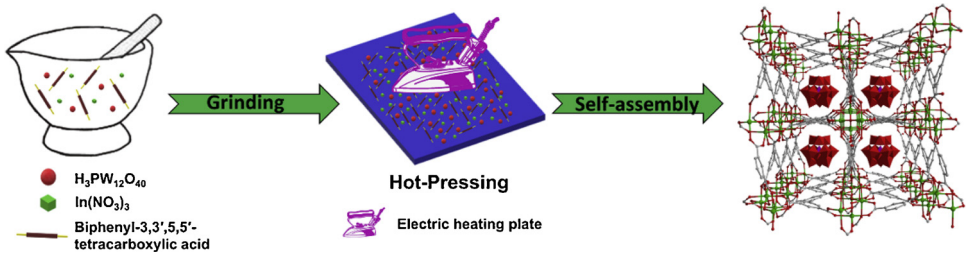

Scheme 1. The hot-pressing synthesis process of PW_{12}@MFM-300(In).

friendly preparation technologies for POM@MOF photocatalysts is emergent and vital.

Herein, we presented an *in-situ* approach to prepare POM@MOF catalyst materials by using a hot-pressing method, in which pressing only 10 min POM can be encapsulated into MOF with high crystallinity and stability. This method is not only solvent-free but also energy/time-saving. In our design, through one-pot solvent-free synthesis, a typical In(III)-based robust MOF, MFM-300(In), was used as a host matrix for the first time to capsulate the $H_3PW_{12}O_{40}$ (PW_{12}) guest to prepare the host-guest PW_{12}@MFM-300(In) composites. In the material, PW_{12} were rapidly and successfully immobilized in the pores of MOF by physical imprisonment. The robustness of this material was investigated by treated with different solutions (CH_3CN, CH_3OH, C_2H_5OH, H_2O and HCl aqueous solution (1 M)). As a novel catalyst, PW_{12}@MFM-300(In) was found very effective for the degradations of PhAC sulfamethazine (SMT) as well as excellent recycling utilization.

2. Experimental

2.1. Materials and general methods

All chemicals are commercially available and were used without further purification. Infrared (IR) spectrum was obtained through an EQUINOX-55 FT-IR spectrometer together with KBr pellet from 4000 to 400 cm^{-1}. Elemental analyses for C, H and N were recorded on a Perkin-Elmer 2400C Elemental Analyzer. Powder X-ray diffraction (PXRD) data was collected on a Bruker D8 ADVANCE with Cu-Kα radiation (λ = 1.5418 Å). UV–vis spectroscopy was measured on a Hitachi U-3310 spectrometer. Inductively coupled plasma (ICP) spectroscopy was performed on an Agilent 725 ICP-OES spectrometer. Gas sorption isotherm was measured by an ASAP 2020 M adsorption equipment. The concentration of SMT was measured by a high-performance liquid chromatography (Shimadzu LCMS-2020). Scanning electron microscopy (SEM) analysis was carried out on an SU8010 Field Emission Scanning Electron Microscope. Transmission electron microscope (TEM) analysis was carried out on a JEOL JEM-2100 Plus Transmission Electron Microscope.

2.2. Synthesis of MFM-300(In)

$In(NO_3)_3{\cdot}5H_2O$ (0.8 mmol, 312 mg) and biphenyl-3,3′,5,5′-tetracarboxylic acid (H_4BPTC, 1.0 mmol, 330 mg) were mixed and manually ground. The mixture was then packed with an aluminum foil and heated with an electric heating plate at 80 °C for 10 min. After peeling off the aluminum foil, the obtained powder was washed with DMF, H_2O and ethanol to afford the MOF. It was pre-dried at 80 °C for 30 min prior to use for characterizations.

2.3. Synthesis of PW_{12}@MFM-300(In)

The preparation procedure of PW_{12}@MFM-300(In) is similar to that of MFM-300(In) except the different amounts of PW_{12} (0.2, 0.4 and 0.6 mmol) were added. Following these steps, a series of PW_{12}@MFM-300(In) composites with the different contents of PW_{12} were obtained, which were denoted as 2-PW_{12}@MFM-300(In), 4-PW_{12}@MFM-300(In) and 6-PW_{12}@MFM-300(In), respectively.

2.4. Catalytic performance

Degradation experiments were carried out in a glass tube (30 ml) with 20 mL SMT solution in a BL-GHX-V photochemical reaction instrument with 160 rpm at room temperature. The pH of initial solution was adjusted by HCl (0.1 M). The known amounts of H_2O_2 and catalysts were added to initiate the reaction. The experiments were carried out three times, and the results were the average value. All samples were filtered with a micro-filtration membrane (0.22 um) before analysis.

3. Result and discussion

3.1. Preparation

MFM-300(In) and PW_{12}@MFM-300(In) were synthesized through a recently reported solvent-free *in-situ* hot-pressing (HoP) method [40], in which the hot pressing under appropriate temperature for a certain time can turn the raw materials of metal sources and ligands into highly stable products. In a typical preparation procedure of MFM-300(In), the powdered mixture of $In(NO_3)_3{\cdot}5H_2O$ and H_4BPTC was put into a zirconia milling pot and ball-milled using zirconia balls for 5 min, the obtained powder was covered with a piece of aluminum foil, and then packed with an electric iron at 80 °C for 10 min. The sample was washed by DMF, H_2O and EtOH (each for five times) to ensure that all the unreacted reactants were removed. For the preparation of PW_{12}@MFM-300(In), only additional appropriate amount of PW_{12} was added in the initial reactants (Scheme 1). To our best knowledge, this facile solvent-free *in-situ* HoP procedure was previously not adopted to synthesize POM@MOF, which avoids the use of polluting organic solvents and is also time/energy-saving. This method also provides an alternative opportunity for a massive production of related materials only by magnifying the preparation container.

3.2. Characterization

The PXRD patterns of different PW_{12}@MFM-300(In) samples are in good agreement with that of MFM-300(In) sample as well as the calculated from the single crystal structure of MFM-300(In) (Fig. 1a), indicating the encapsulation of PW_{12} without altering the cell parameters of MFM-300(In). The diffraction peaks of PW_{12} are not easily distinguished, suggesting that PW_{12} are mainly encaged in the pores of MFM-300(In) and no aggregated PW_{12} particles were formed during the synthesis process [41]. The characteristic bands of both PW_{12} and MFM-300(In) can be observed in the IR spectra of PW_{12}@MFM-300(In) (Fig. 1b). The peaks between 850 and 1100 cm^{-1} are assigned to the P-O and W-O vibrations of PW_{12}, while those between 1300 and 1600 cm^{-1} are attributed to the carboxylate vibrations of MFM-300(In) [27,38]. This fact illustrated the presence of PW_{12} in PW_{12}@MFM-300(In). The successful capsulation of PW_{12} in MFM-300(In) was further demonstrated by the N_2 adsorption analysis performed at 77 K. It shows that the increase of PW_{12} content in PW_{12}@MFM-300(In) leads to a gradual

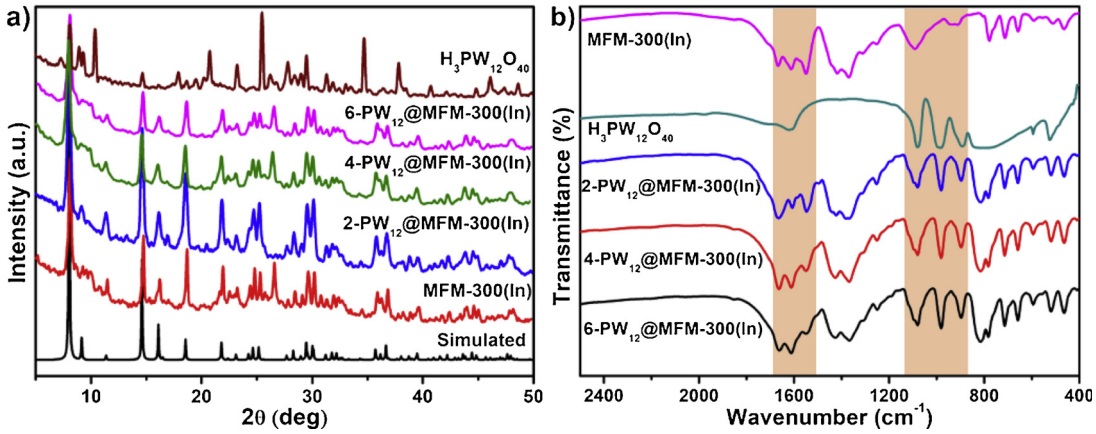

Fig. 1. a) Powder XRD patterns and b) FT-IR spectra of the samples.

decrease of Brunauer-Emmett-Teller (BET) surface area, resulting from the pores of MFM-300(In) occupied by different amounts of PW_{12} molecules (Fig. S1).

To uncover the microscopic structure of composites, 4-PW_{12}@MFM-300(In) was selected as a representative material. SEM analysis reveals that 4-PW_{12}@MFM-300(In) consists of intergrowth block micro-crystals with the particle diameter of about 100–300 nm (Fig. 2a). Meanwhile, TEM result shows no PW_{12} aggregates on the surface of 4-PW_{12}@MFM-300(In) (Fig. 2b), implying that the PW_{12} molecules are probably encapsulated in MFM-300(In) rather than adhered to the surface of MFM-300(In). This situation was similar to other reported POM@MOF systems [42,43]. Furthermore, the EDX analysis of 4-PW_{12}@MFM-300(In) at randomly selected areas detected the presence of W and P elements (Fig. 2c), which can also be clearly reflected by the EDX elemental mappings (Fig. 2d). The low densities of P and W relative to that of In agree with their calculated contents. Based on the ICP-AES results of the acidic piranha-digested sample of 4-PW_{12}@MFM-300(In), the W: In molar ratio of 1:4.3 was calculated.

Above characterization results indicated the successful confinement of PW_{12} into the pores of MFM-300(In) during the HoP preparing process. The interactions of POM and MOF in 4-PW_{12}@MFM-300(In) were also investigated by spectroscopic methods. Compared to the UV–vis spectrum of MFM-300(In), the absorption edge of 4-PW_{12}@MFM-300(In) is extended to 450 nm, and a new absorption band ranging from 550 to 600 nm is also observed (Fig. 3a). This new absorption band is possibly attributed to the charge transfer between O atoms in PW_{12} and In(III) ions in MFM-300(In), as reported in the recently published work [39]. At the same time, the presence of PW_{12} significantly decreases the light harvesting ability of 4-PW_{12}@MFM-300(In) with an obviously decreased fluorescence at an excitation of 340 nm (Fig. 3b), also illustrating an efficient electron transfer between PW_{12} and MFM-300(In). This would create a favourable environment for the synergistic photocatalytic activity of 4-PW_{12}@MFM-300(In).

XPS analysis on 4-PW_{12}@MFM-300(In) was performed to further analyze the interactions between PW_{12} and MFM-300(In), and the characteristic peaks corresponding to In 3d, W 4f, P 2p, O 1s, and C 1s were found (Fig. 3c). The high resolution of In 3d XPS spectra of both MFM-300(In) and 4-PW_{12}@MFM-300(In) were presented in Fig. 3d, which displays a slight shift to a higher binding energy in 4-PW_{12}@MFM-300(In) compared to pure MFM-300(In). This change may be caused by the interactions between PW_{12} and MFM-300(In) host in 4-PW_{12}@MFM-300(In), in which the O atoms in PW_{12} possibly interact with the oxophilic In(III) ions in MFM-300(In). Such a shift also reflects the decrease of the electron density around the indium atoms, and suggests the electron transfer occurred from MFM-300(In) to PW_{12} [9,44,45].

3.3. Photocatalytic properties

The photocatalytic activity of PW_{12}@MFM-300(In) was evaluated via decomposing SMT that is one of the most refractory PhACs [46,47]. The degradation experiments were performed under various conditions

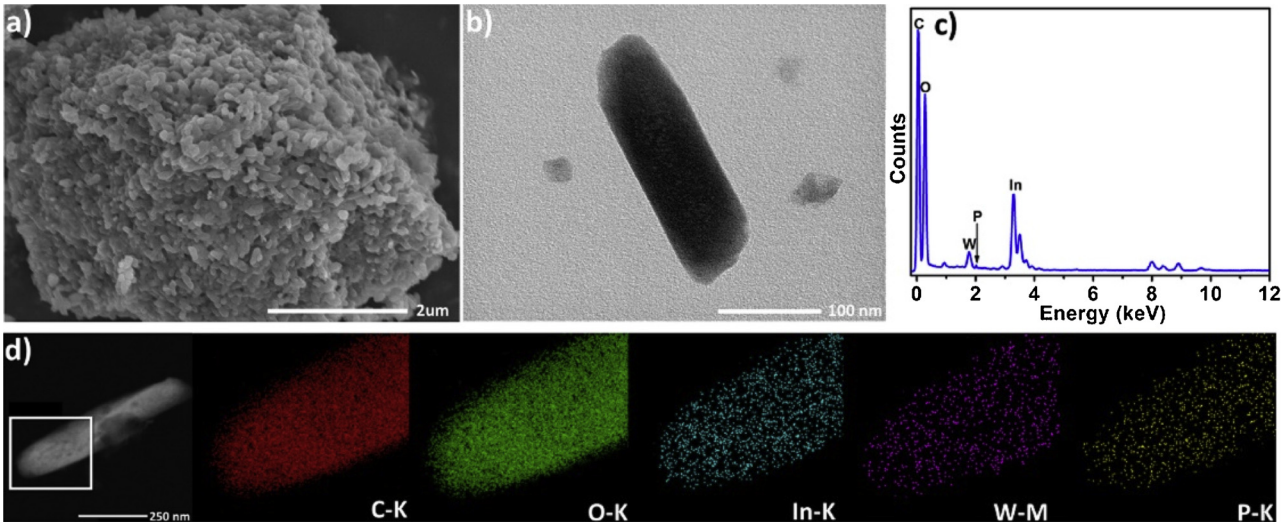

Fig. 2. a) SEM image of 4-PW_{12}@MFM-300(In); b) TEM image of 4-PW_{12}@MFM-300(In); c) EDX and d) mapping images of 4-PW_{12}@MFM-300(In).

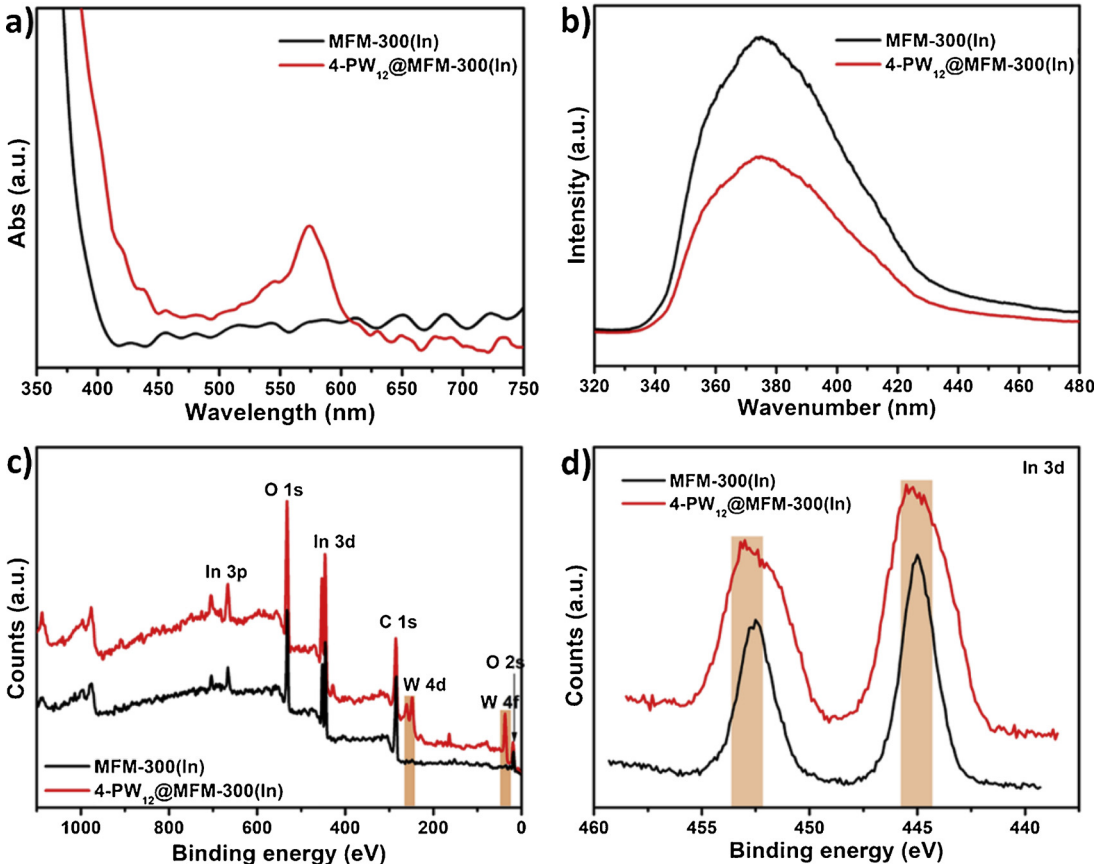

Fig. 3. a) Diffuse reflectance UV–vis spectra and b) emission spectra (λ_{ex} = 340 nm) of MFM-300(In) and 4-PW_{12}@MFM-300(In); c) Survey XPS spectra and d). high-resolution In 3d XPS spectra of MFM-300(In) and 4-PW_{12}@MFM-300(In).

of pH and H_2O_2 concentrations, catalyst dosages and types (including MFM-300(In), PW_{12}, and different composites of 2-PW_{12}@MFM-300(In), 4-PW_{12}@MFM-300(In) and 6-PW_{12}@MFM-300(In)). Fig. 4a shows the degradation profiles of SMT under different systems, which indicates a very limited degradation efficiency of SMT for the single utilization of H_2O_2 (2.1%) or MFM-300(In) (53.6%). In contrast, the PW_{12}@MFM-300(In) composites have significantly enhanced photocatalytic degradation performance (> 90%) toward SMT. In particular, 4-PW_{12}@MFM-300(In) reveals the highest degradation efficiency of 98.0% after 2 h under the presence of H_2O_2. 4-PW_{12}@MFM-300(In) also possesses a certain catalytic activity toward SMT in dark, but with the obviously lower efficiency. The high catalytic efficiency in PW_{12}@MFM-300(In) was attributed to the following reasons: 1) together with large specific surface areas and regular porous structure of MOF host, PW_{12} can be uniformly distributed in the pores of MOF; 2) the existing metal sites and/or organic fragments in the pores can induce region-selectivity toward H_2O_2, thereby improving accessibility of H_2O_2 to the active sites; 3) the composite structure of PW_{12}@MFM-300(In) promotes the host-guest electron transfers, contributing to a high catalytic efficiency. Meanwhile, the excess amount of PW_{12} in MFM-300(In), such as for 6-PW_{12}@MFM-300(In), induces a decreased photocatalytic performance due to the reduction of accessible active sites in MOF. Therefore, a synergistic effect between PW_{12} and MFM-300(In) is crucial to improve the photoactivity of composite.

Due to better efficiency of 4-PW_{12}@MFM-300(In) toward SMT degradation compared to other two composites, the catalytic performance of 4-PW_{12}@MFM-300(In) was further estimated by altering other factors, such as catalyst dosage, pH and H_2O_2 concentration. As shown in Fig. 4b, the increase of catalyst dosage greatly accelerated SMT degradation. When the dosage increased from 0.3 to 0.9 g/L, the catalytic rate was significantly improved, while the catalytic efficiency was raised slightly. This result originates from the fact that the increased catalyst dosage provides more active sites to produce $^{\cdot}OH$ radicals through forming more contacts between catalyst and H_2O_2.

The influence of solution acidity on the photocatalytic process in 4-PW_{12}@MFM-300(In) was also investigated. As shown in Fig.4c, the pH plays an important role in the whole process and the optimal pH was about 6.0. This phenomenon can be explained by measuring point-of-zero charge (pH_{pzc}) of the material, which was found to be about 5.8 (Fig. S2). Namely, when the solution pH ≥ pH_{pzc} or pH ≤ pH_{pzc}, the catalyst had negative charge or positive charge, respectively. As the pK_a of SMT molecules is pK_{a1} = 2.28, and pK_{a2} = 7.42 (Fig. S3) [44], in the case of the solution pH ≥ pK_{a2}, pH ≤ pK_{a1} or pK_{a1} ≤ pH ≤ pK_{a2}, the SMT molecules exist as anions, cations or zwitterions, respectively. The adsorption is considered to be a crucial step during the process of photodegradation, the working pH range of catalyst (pH_{pzc} = 5.8) falling in 2.28–7.42 is beneficial for adsorbing anionic and cationic groups in SMT molecules. However, when the solution pH range is out of 2.28–7.42, the adsorption function will be inhibited because of electro-static repulsion.

In addition, the H_2O_2 concentration also moderately affects the catalytic efficiency of 4-PW_{12}@MFM-300(In). As illustrated in Fig. 4d, with the increase of H_2O_2 concentration from 3.0 to 12.0 mM, the removal efficiency of SMT is firstly increased until at a concentration of 6.0 mM and then decreased. Thus, the effect of H_2O_2 on the SMT degradation is dual. With the increase of H_2O_2 concentration, more $^{\cdot}OH$ radicals were generated to degrade high concentration of SMT, but the excess H_2O_2 was also regarded as a scavenger of $^{\cdot}OH$ radical. Meanwhile, the competitive adsorption between H_2O_2 and SMT is also an adverse factor. So an optimal H_2O_2 concentration of 6.0 mM is available for the best degradation efficiency of SMT.

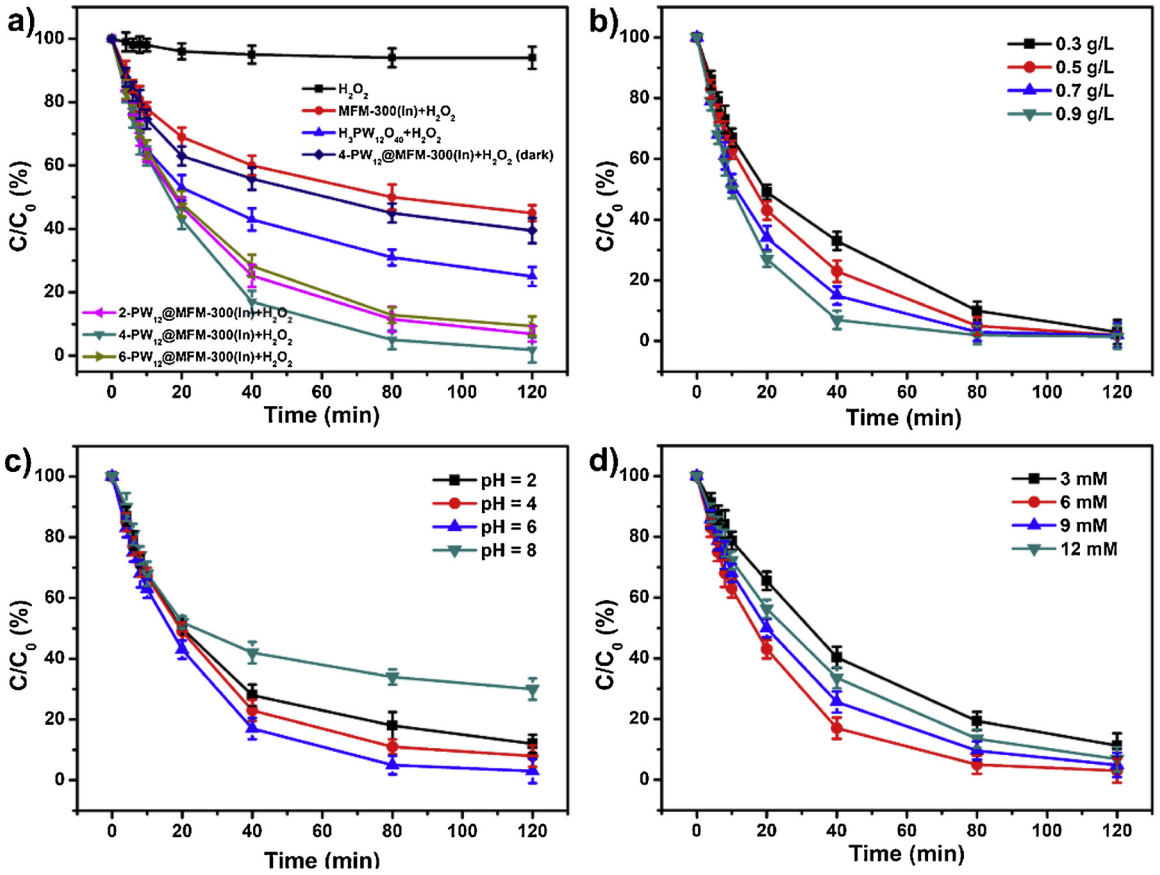

Fig. 4. a) Degradation of SMT with different catalysts; b), c) and d) photocatalytic degradation of SMT over 4-PW_{12}@MFM-300(In) at different catalyst dosages, different pH and different H_2O_2 concentrations, respectively. Except for the investigated parameter, other parameters fixed on H_2O_2 = 6.0 mM, different PW_{12}@MFM-300(In) composites = 0.6 g/L, pH = 6, 40 mL SMT = 0.06 mmol/L and room temperature.

3.4. Stability and reusability

The robustness of catalytic materials is one of the critical prerequisite in practical application under harsh condition. When 4-PW_{12}@MFM-300(In) was treated with various solvents, PXRD date confirmed the structural intactness of material (Fig. S4). Moreover, the UV–vis spectra suggested no PW_{12} leached out from the MOF (Fig. S5). The good chemical stability of 4-PW_{12}@MFM-300(In) is probably due to strong POM-MOF interactions from the complementary shape [29,41]. To further evaluate the cyclic stability of catalyst, eight times of successive experiments were carried out under the same condition. And a high SMT degradation efficiency (85%) is still reached after eight times of experiments (Fig. 5). PXRD confirmed the integrate structure of 4-PW_{12}@MFM-300(In) after eight consecutive cycles (Fig. S6).

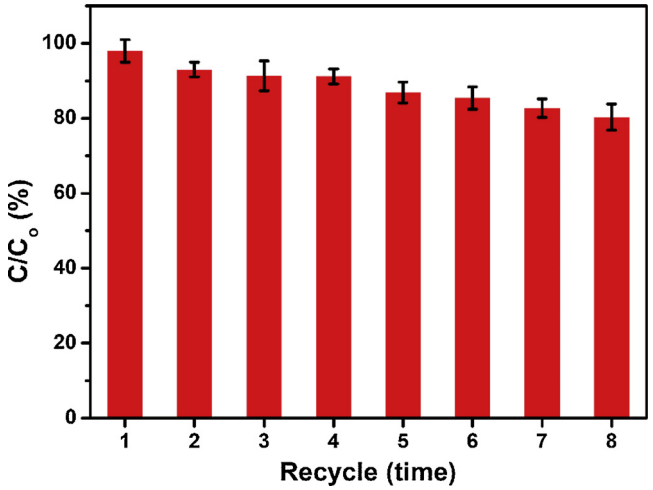

Fig. 5. Recyclability study of 4-PW_{12}@MFM-300(In) catalyst.

3.5. Catalytic mechanism

The mechanism of the photocatalytic activity of 4-PW_{12}@MFM-300(In) was further analyzed. The indium-oxygen clusters and the organic bridging ligands of MOF host in PW_{12}@MFM-300(In) can behave as quantum dots and antennas, respectively. Under visible light, the ligands harvest visible light and then transfer energy to inorganic indium-oxygen cluster part. Subsequently, the photogenerated electrons from MFM-300(In) rapidly migrate to the conduction bond (CB) of PW_{12}, resulting in efficient carrier separation and thus an enhanced photocatalytic activity. Consequently, the obtained photogenerated electrons are captured by H_2O_2 to form $^{\cdot}OH$ radicals, which possess a strong capacity to oxidize organic molecules. Meanwhile, the photogenerated holes oxidize the hole scavengers to form more $^{\cdot}OH$, thus greatly enhancing the efficiency of SMT degradation. (Eqs. (1)–(3)).

$$PW_{12}@MFM-300(In) \xrightarrow{h\nu} PW_{12}@MFM-300(In)\,(h^+ + e^-) \quad (1)$$

$$e^- + H_2O_2 \rightarrow {}^{\cdot}OH + OH^- \quad (2)$$

$$h^+ + H_2O \rightarrow {}^{\cdot}OH + H^+ \quad (3)$$

Taking account of the product distribution in the current catalytic system (Fig. S7) and the related literatures (Table S1) [3,8,48–51], we proposed the reaction pathways for the SMT degradation by catalysts, as shown in Scheme 2. The active species, holes, $^{\cdot}OH$ could selectively degrade the target pollutant (SMT) into more intermediates or directly

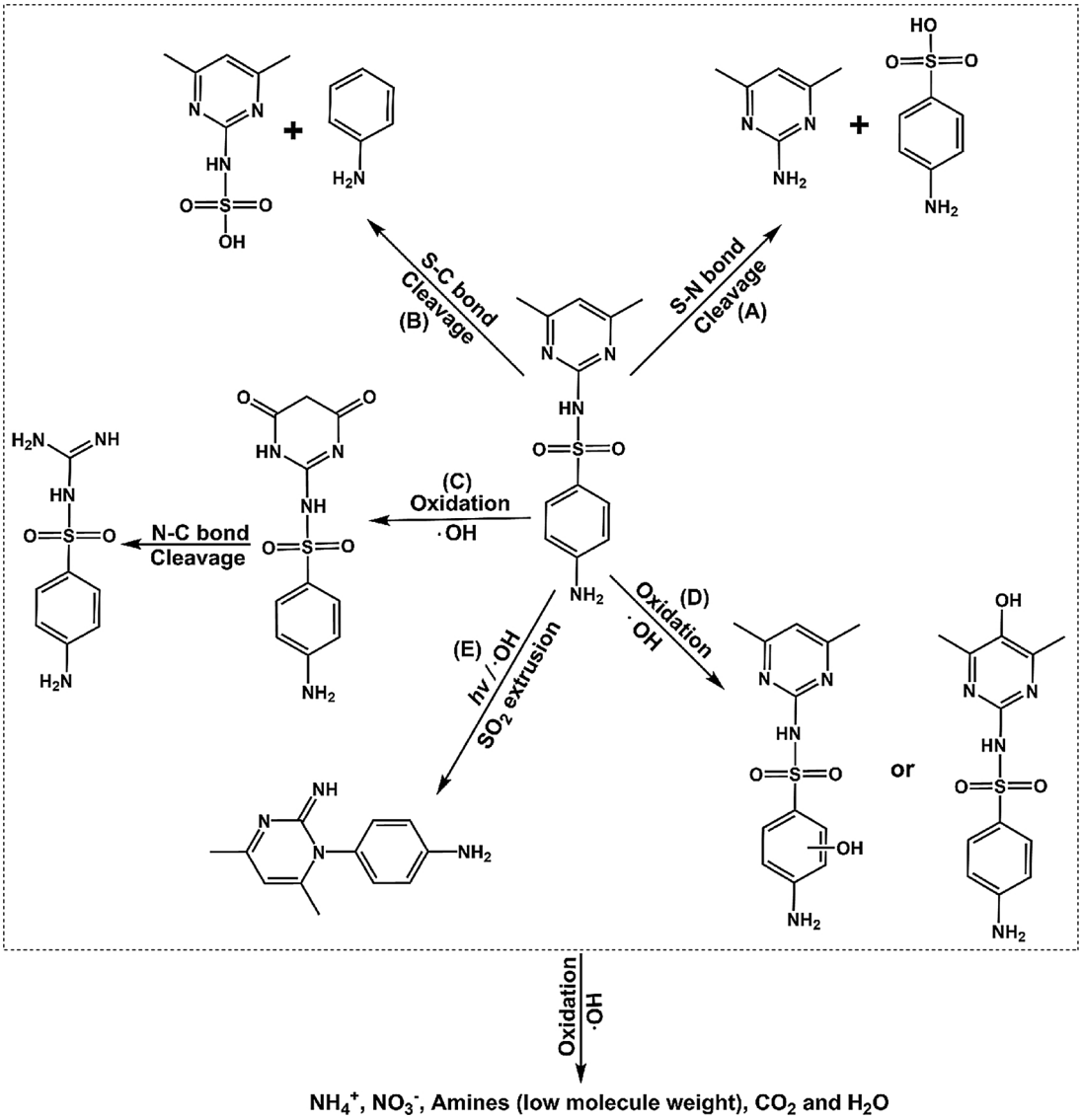

Scheme 2. Possible pathways of SMT degradation.

into end products (NH_4^+, NO_3^-, CO_2, H_2O and amines) [3,8,52]. The cleavage of N–S bond in SMT was supposed to be the main pathway for SMT degradation to produce sulfanilic acid and 2-amino-4,6-dimethylpyrimidine (pathway A) [8]. The (4,6-dimethylpyrimidin-2-yl) sulfamic acid and 4-amino-*N*-carbamimidoylbenzenesulfonamide were also produced, which resulted from the cleavages of S—C and N—C bonds (pathway B and C) [3,8,46]. During the process, H-abstract and ·OH radical oxidation occurred. Meanwhile, the ·OH-mediated oxidation of SMT produced hydroxylated sulfamethazine (pathway D) [3] and the products continued to be degraded. In addition, SO_2 elimination driven by UV direct photolysis or ·OH is also another possible degradation pathway (pathway E) [46,47,53]. With continuing ·OH oxidation, the intermediates would be oxidized into NH_4^+, NO_3^-, CO_2 and H_2O [3,8].

4. Conclusions

In summary, an unprecedented solvent-free hot-pressing strategy has been demonstrated to be a green synthesis method to incorporate PW_{12} into MFM-300(In) by physical imprisonment, giving rise to a robust host-guest POM@MOF photocatalyst with high loading efficiency. SMT degradation experiments demonstrated a 98% degradation efficiency was achieved under optimal conditions (pH = 6, T = 35 °C, H_2O_2 = 6 mM) via using 4-PW_{12}@MFM-300(In) material as an heterogeneous catalyst. The robust 4-PW_{12}@MFM-300(In) catalyst displays good chemical stability towards different acid and organic solvent systems as well as good regeneration and reusability. These advantages enable 4-PW_{12}@MFM-300(In) to be an excellent catalyst candidate applied to the SMT degradation in water. This presentation not only offers new insight into strategy for the design and fabrication of POM@MOF photocatalysts by an environment-friendly synthesis method, but also provides a simple and highly efficient route to degrade sulfamethazine pollutant in water by using POM@MOF photocatalysts under visible light irradiation.

Acknowledgements

This work was supported by the National Natural Science Foundation of China (Grants 21531007, 21871220 and 21875187), the Natural Science Basic Research Plan in Shaanxi Province of China (Program No. 2018JQ2026 and 2017JQ2012) and Scientific Research Program Funded by Shaanxi Provincial Education Department (Program No. 18JK0355). Thanks are due to Mr. Zijun Ren and Ms. Jiao Li for their valuable technical support.

Appendix A. Supplementary data

Supplementary material related to this article can be found, in the online version, at doi:https://doi.org/10.1016/j.apcatb.2019.01.012.

References

[1] Q. Yan, G. Feng, X. Gao, C. Sun, J.S. Guo, Z. Zhu, Removal of pharmaceutically active compounds (PhACs) and toxicological response of Cyperus alternifolius exposed to PhACs in microcosm constructed wetlands, J. Hazard. Mater. 301 (2016) 566–575.

[2] V. Rakic, V. Rac, M. Krmar, O. Otman, A. Auroux, The adsorption of pharmaceutically active compounds from aqueous solutions onto activated carbons, J. Hazard. Mater. 282 (2015) 141–149.

[3] Z. Wan, J. Wang, Degradation of sulfamethazine using Fe_3O_4-Mn_3O_4/reduced graphene oxide hybrid as Fenton-like catalyst, J. Hazard. Mater. 324 (2017) 653–664.

[4] X. Peng, Z. Wang, W. Kuang, J. Tan, K. Li, A preliminary study on the occurrence and behavior of sulfonamides, ofloxacin and chloramphenicol antimicrobials in wastewaters of two sewage treatment plants in Guangzhou, China, Sci. Total Environ. 371 (2006) 314–322.

[5] N. Le-Minh, S.J. Khan, J.E. Drewes, R.M. Stuetz, Fate of antibiotics during municipal water recycling treatment processes, Water Res. 44 (2010) 4295–4323.

[6] R.H. Lindberg, P. Wennberg, M.I. Johansson, M. Tysklind, B.A.V. Andersson, Screening of human antibiotic substances and determination of weekly mass flows in five sewage treatment plants in Sweden, Environ. Sci. Technol. 39 (2005) 3421–3429.

[7] M. Taheran, S.K. Brar, M. Verma, R.Y. Surampalli, T.C. Zhang, J.R. Valero, Membrane processes for removal of pharmaceutically active compounds (PhACs) from water and wastewaters, Sci. Total Environ. 547 (2016) 60–77.

[8] Y. Liu, J. Wang, Degradation of sulfamethazine by gamma irradiation in the presence of hydrogen peroxide, J. Hazard. Mater. 250 (2013) 99–105.

[9] J. Qiu, X. Zhang, Y. Feng, X. Zhang, H. Wang, J. Yao, Modified metal-organic frameworks as photocatalysts, Appl. Catal. B: Environ. 231 (2018) 317–342.

[10] J. Shi, Y. Kuwahara, M. Wen, M. Navlani-Garcia, K. Mori, T. An, H. Yamashita, Room-temperature and aqueous-phase synthesis of plasmonic molybdenum oxide nanoparticles for visible-light-enhanced hydrogen generation, Chem. Asian J. 11 (2016) 2377–2381.

[11] Y. Ye, Z. Zang, T. Zhou, F. Dong, S. Lu, X. Tang, W. Wei, Y. Zhang, Theoretical and experimental investigation of highly photocatalytic performance of CuInZnS nanoporous structure for removing the NO gas, J. Catal. 357 (2018) 100–107.

[12] P. Wu, Z. Xiao, J. Zhang, J. Hao, J. Chen, P. Yin, Y. Wei, DMAP-catalyzed esterification of pentaerythritol-derivatized POMs: a new route for the functionalization of polyoxometalates, Chem. Commun. (Camb.) 47 (2011) 5557–5559.

[13] I.V. Kozhevnikov, Catalysis by heteropoly acids and multicomponent polyoxometalates in liquid-phase reactions, Chem. Rev. 98 (1998) 171–198.

[14] S. Chakraborty, A. Keightley, V. Dusevich, Y. Wang, Z. Peng, Synthesis and Optical properties of a rod−coil diblock copolymer with polyoxometalate clusters covalently attached to the coil block, Chem. Mater. 22 (2010) 3995–4006.

[15] G. Ferey, Hybrid porous solids: past, present, future, Chem. Soc. Rev. 37 (2008) 191–214.

[16] J.R. Long, O.M. Yaghi, The pervasive chemistry of metal-organic frameworks, Chem. Soc. Rev. 38 (2009) 1213–1214.

[17] M. Misono, Heterogeneous catalysis by heteropoly compounds of molybdenum and tungsten, Catal. Rev.-Sci. Eng. 29 (1987) 269–321.

[18] D.-Y. Du, J.-S. Qin, S.-L. Li, Z.-M. Su, Y.-Q. Lan, Recent advances in porous polyoxometalate-based metal-organic framework materials, Chem. Soc. Rev. 43 (2014) 4615–4632.

[19] H. Yang, J. Li, H. Zhang, Y. Lv, S. Gao, Facile synthesis of POM@MOF embedded in SBA-15 as a steady catalyst for the hydroxylation of benzene, Microporous Mesoporous Mater. 195 (2014) 87–91.

[20] S.-W. Li, R.-M. Gao, R.-L. Zhang, J.-s. Zhao, Template method for a hybrid catalyst material POM@MOF-199 anchored on MCM-41: highly oxidative desulfurization of DBT under molecular oxygen, Fuel 184 (2016) 18–27.

[21] R.R. Ozer, J.L. Ferry, Photocatalytic oxidation of aqueous 1,2-dichlorobenzene by polyoxometalates supported on the NaY zeolite, J. Phys. Chem. B 106 (2002) 4336–4342.

[22] S. Xu, L. You, P. Zhang, Y. Zhang, J. Guo, C. Wang, Fe_3O_4@coordination polymer microspheres with self-supported polyoxometalates in shells exhibiting high-performance supercapacitive energy storage, Chem. Commun. (Camb.) 49 (2013) 2427–2429.

[23] Y. Leng, J. Wang, D. Zhu, X. Ren, H. Ge, L. Shen, Heteropolyanion-based ionic liquids: reaction-induced self-separation catalysts for esterification, Angew. Chem. Int. Ed. Engl. 48 (2009) 168–171.

[24] J. Hu, K. Li, W. Li, F. Ma, Y. Guo, Selective oxidation of styrene to benzaldehyde catalyzed by Schiff base-modified ordered mesoporous silica materials impregnated with the transition metal-monosubstituted Keggin-type polyoxometalates, Appl. Catal. A Gen. 364 (2009) 211–220.

[25] Y. Xu, T. Liu, Y. Zhang, F. Ge, R.M. Steel, L. Sun, Advances in technologies for pharmaceuticals and personal care products removal, J. Mater. Chem. A Mater. Energy Sustain. 5 (2017) 12001–12014.

[26] M. Wen, K. Mori, Y. Kuwahara, H. Yamashita, Plasmonic Au@Pd nanoparticles supported on a basic metal-organic framework: synergic boosting of H_2 production from formic acid, ACS Energy Lett. 2 (2017) 1–7.

[27] Design and architecture of metal organic frameworks for visible light enhanced hydrogen production, Appl. Catal. B: Environ. 218 (2017) 555–569.

[28] Y.T. Xu, X. Xiao, Z.M. Ye, S. Zhao, R. Shen, C.T. He, J.P. Zhang, Y. Li, X.M. Chen, Cage-confinement pyrolysis route to ultrasmall tungsten carbide nanoparticles for efficient electrocatalytic hydrogen evolution, J. Am. Chem. Soc. 139 (2017) 5285–5288.

[29] S. Mukhopadhyay, J. Debgupta, C. Singh, A. Kar, S.K. Das, A. Keggin, Polyoxometalate shows water oxidation activity at neutral pH: pom@zif-8, an efficient and robust electrocatalyst, Angew. Chem. Int. Ed. 57 (2018) 1918–1923.

[30] W. Guo, H. Lv, Z. Chen, K.P. Sullivan, S.M. Lauinger, Y. Chi, J.M. Sumliner, T. Lian, C.L. Hill, Self-assembly of polyoxometalates, Pt nanoparticles and metal–organic frameworks into a hybrid material for synergistic hydrogen evolution, J. Mater. Chem. A Mater. Energy Sustain. 4 (2016) 5952–5957.

[31] Y.-L. Peng, J. Liu, H.-F. Zhang, D. Luo, D. Li, A size-matched POM@MOF composite catalyst for highly efficient and recyclable ultra-deep oxidative fuel desulfurization, Inorg. Chem. Front. 5 (2018) 1563–1569.

[32] J. Zhao, W.-W. Dong, Y.-P. Wu, Y.-N. Wang, C. Wang, D.-S. Li, Q.-C. Zhang, Two (3,6)-connected porous metal–organic frameworks based on linear trinuclear $[Co_3(COO)_6]$ and paddlewheel dinuclear $[Cu_2(COO)_4]$ SBUs: gas adsorption, photocatalytic behaviour, and magnetic properties, J. Mater. Chem. A Mater. Energy Sustain. 3 (2015) 6962–6969.

[33] H.-R. Fu, L.-B. Yan, N.-T. Wu, L.-F. Ma, S.-Q. Zang, Dual-emission MOF⊃dye sensor for ratiometric fluorescence recognition of RDX and detection of a broad class of nitro-compounds, J. Mater. Chem. A Mater. Energy Sustain. 6 (2018) 9183–9191.

[34] J. Liu, G. Liu, C. Gu, W. Liu, J. Xu, B. Li, W. Wang, Rational synthesis of a novel 3,3,5-c polyhedral metal-organic framework with high thermal stability and hydrogen storage capability, J. Mater. Chem. A Mater. Energy Sustain. 4 (2016) 11630–11634.

[35] X.-L. Luo, Z. Yin, M.-H. Zeng, M. Kurmoo, The construction, structures, and functions of pillared layer metal-organic frameworks, Inorg. Chem. Front. 3 (2016) 1208–1226.

[36] M. Zhang, W. Zhou, T. Pham, K.A. Forrest, W. Liu, Y. He, H. Wu, T. Yildirim, B. Chen, B. Space, Y. Pan, M.J. Zaworotko, J. Bai, Fine tuning of MOF-505 analogues to reduce low-pressure methane uptake and enhance methane working capacity, Angew.Chem. Int. Ed. 56 (2017) 11426–11430.

[37] M. Du, C.P. Li, M. Chen, Z.W. Ge, X. Wang, L. Wang, C.S. Liu, Divergent kinetic and thermodynamic hydration of a porous Cu(II) coordination polymer with exclusive CO_2 sorption selectivity, J. Am. Chem. Soc. 136 (2014) 10906–10909.

[38] R.-W. Huang, Y.-S. Wei, X.-Y. Dong, X.-H. Wu, C.-X. Du, S.-Q. Zang, T.C.W. Mak, Hypersensitive dual-function luminescence switching of a silver-chalcogenolate cluster-based metal-organic framework, Nat. Chem. 9 (2017) 689–697.

[39] C.T. Buru, A.E. Platero-Prats, D.G. Chica, M.G. Kanatzidis, K.W. Chapman, O.K. Farha, Thermally induced migration of a polyoxometalate within a metal–organic framework and its catalytic effects, J. Mater. Chem. A Mater. Energy Sustain. 6 (2018) 7389–7394.

[40] Y. Chen, S. Li, X. Pei, J. Zhou, X. Feng, S. Zhang, Y. Cheng, H. Li, R. Han, B. Wang, A solvent-free hot-pressing method for preparing metal–organic-framework coatings, Angew.Chem. Int. Ed. 55 (2016) 3419–3423.

[41] X. Zhao, Y. Duan, F. Yang, W. Wei, Y. Xu, C. Hu, Efficient mechanochemical synthesis of polyoxometalate subset ZIF complexes as reusable catalysts for highly selective oxidation, Inorg. Chem. 56 (2017) 14506–14512.

[42] R. Liang, R. Huang, S. Ying, X. Wang, G. Yan, L. Wu, Facile in situ growth of highly dispersed palladium on phosphotungstic-acid-encapsulated MIL-100(Fe) for the degradation of pharmaceuticals and personal care products under visible light, Nano Res. 11 (2017) 1109–1123.

[43] X.-S. Wang, L. Li, J. Liang, Y.-B. Huang, R. Cao, Boosting oxidative desulfurization of model and real gasoline over phosphotungstic acid encapsulated in metal-organic frameworks: the window size matters, ChemCatChem 9 (2017) 971–979.

[44] M. Teixidó, J.J. Pignatello, J.L. Beltrán, M. Granados, J. Peccia, Speciation of theionizable antibiotic sulfamethazine on black carbon (biochar), Environ. Sci. Technol. 45 (2011) 10020–10027.

[45] W. Zhou, T. Xiong, C. Shi, J. Zhou, K. Zhou, N. Zhu, L. Li, Z. Tang, S. Chen, Bioreduction of precious metals by microorganism: efficient gold@N-doped carbon electrocatalysts for the hydrogen evolution reaction, Angew. Chem. Int. Ed. Engl. 55 (2016) 8416–8420.

[46] Y.-q. Gao, N.-y. Gao, Y. Deng, Y.-q. Yang, Y. Ma, Ultraviolet (UV) light-activated persulfate oxidation of sulfamethazine in water, Chem. Eng. J. 195-196 (2012) 248–253.

[47] M. Li, C. Wang, M. Yau, J.R. Bolton, Z. Qiang, Sulfamethazine degradation in water by the VUV/UV process: kinetics, mechanism and antibacterial activity determination based on a mini-fluidic VUV/UV photoreaction system, Water Res. 108 (2017) 348–355.

[48] Y. Fan, Y. Ji, D. Kong, J. Lu, Q. Zhou, Kinetic and mechanistic investigations of the degradation of sulfamethazine in heat-activated persulfate oxidation process, J. Hazard. Mater. 300 (2015) 39–47.

[49] S.M. Mitchell, J.L. Ullman, A.L. Teel, R.J. Watts, C. Frear, The effects of the antibiotics ampicillin, florfenicol, sulfamethazine, and tylosin on biogas production and their degradation efficiency during anaerobic digestion, Bioresour. Technol. 149 (2013) 244–252.

[50] M. Perez-Moya, M. Graells, G. Castells, J. Amigo, E. Ortega, G. Buhigas, L.M. Perez, H.D. Mansilla, Characterization of the degradation performance of the sulfamethazine antibiotic by photo-Fenton process, Water Res. 44 (2010) 2533–2540.

[51] Z. Wan, J. Wang, Fenton-like degradation of sulfamethazine using Fe_3O_4/Mn_3O_4 nanocomposite catalyst: kinetics and catalytic mechanism, Environ. Sci. Pollut. Res. Int. 24 (2017) 568–577.

[52] K. Li, L. Yan, Z. Zeng, S. Luo, X. Luo, X. Liu, H. Guo, Y. Guo, Fabrication of $H_3PW_{12}O_{40}$-doped carbon nitride nanotubes by one-step hydrothermal treatment strategy and their efficient visible-light photocatalytic activity toward representative aqueous persistent organic pollutants degradation, Appl. Catal. B: Environ. 156-157 (2014) 141–152.

[53] A.L. Boreen, W.A. Arnold, K. Mcneill, Riplet-sensitized photodegradation of sulfa drugs containing six-membered heterocyclic groups: identification of an SO_2 extrusion photoproduct, Environ. Sci. Technol. 39 (2005) 3630–3638.